Title

Pre-treatment and real-time image guidance for a fixed-beam radiotherapy system

Running title

Image guidance for a fixed-beam radiotherapy system

Authors

Paul Z. Y. Liu[1], Mark Gardner[1], Soo Min Heng[2], Chun-Chen Shieh[1], Doan Trang Nguyen[1,3], Emily Debrot[1], Ricky O'Brien[1], Simon Downes[2], Michael Jackson[2], Paul J. Keall[1]

[1] ACRF Image X Institute, University of Sydney Central Clinical School, Sydney, NSW, Australia

[2] Nelune Comprehensive Cancer Centre, Prince of Wales Hospital, Randwick, NSW, Australia

[3] School of Biomedical Engineering, Faculty of Engineering and IT, University of Technology, Sydney, NSW, Australia

Corresponding email: paul.liu@sydney.edu.au

Mailing address:

ACRF Image X Institute, Biomedical Building

1 Central Ave, Eveleigh, NSW, Australia 2015

Abstract

Purpose: A radiotherapy system with a fixed treatment beam and a rotating patient positioning system could be smaller, more robust and more cost effective compared to conventional rotating gantry systems. However, patient rotation could cause anatomical deformation and compromise treatment delivery. In this work, we demonstrate an image-guided treatment workflow with a fixed beam prototype system that accounts for deformation during rotation to maintain dosimetric accuracy.

Methods: The prototype system consists of an Elekta Synergy linac with the therapy beam orientated directly downward and a custom-built patient rotation system (PRS). A phantom that deforms with rotation was constructed and rotated within the PRS to quantify the performance of two image guidance techniques: motion compensated cone-beam CT for pre-treatment volumetric imaging and Kilovoltage Infraction Monitoring (KIM) for real-time image guidance. The phantom was also irradiated with a 3D conformal beam to evaluate the dosimetric accuracy of the workflow.

Results: The motion compensated cone-beam CT was used to verify pre-treatment position and the average calculated position within -0.3 ± 1.1 mm of the phantom's ground truth position at 0°. KIM tracked the position of the target in real-time as the phantom was rotated and the average calculated position was within -0.2 ± 0.8 mm of the phantom's ground truth position. A 3D conformal treatment delivered on the prototype system with image guidance had a 3%/2 mm gamma pass rate of 96.3% compared to 98.6% delivered using a conventional rotating gantry linac.

Conclusions: In this work, we have shown that image guidance can be used with fixed-beam treatment systems to measure and account for changes in target position to maintain dosimetric coverage during horizontal rotation. This treatment modality could provide a viable treatment option when there is not enough space for a conventional linear accelerator or where the cost is prohibitive.

Keywords

fixed-beam radiotherapy system, image guidance, real-time

Introduction

Radiotherapy is a fundamental part of cancer treatment[1], however there is a critical shortage in the number of linacs around the world. This global shortfall is caused in part by the large capital requirements, operation costs and staffing required to set up and maintain a treatment facility which disproportionately affects low-to-middle income countries[2-4]. Fixed-beam treatment systems remove the need to rotate the heavy components of the gantry with high precision and are often used in proton or heavy ion therapy where gantry rotation is impractical[5,6]. In order to achieve the desired beam position and angle, fixed-beam systems are usually integrated with patient positioning systems, for example a 6 degree-of-freedom robotic couch. The same concept can be applied to x-ray systems to reduce the size, complexity and footprint relative to conventional rotating gantry linacs. Such systems enable a simplified linac design and can potentially improve global access to radiotherapy.[7]

We have previously developed a prototype compact fixed-beam system that utilizes a vertical radiation beam with horizontal patient rotation (Figure 1). The prototype consists of an Elekta Synergy linac integrated with a bespoke patient rotation system (PRS). The design and characterization of the PRS has been described in Feain *et al.*[8] and the development and commissioning of the prototype system has been described in Liu *et al.*[9] During commissioning, the fixed-beam prototype system was demonstrated to deliver 3D conformal treatments with the same level of geometric and dosimetric accuracy as conventional rotating gantry linacs, however, this was tested on rigid phantoms immobilized within the PRS. Rigid phantoms do not replicate the conditions of patient treatments, where a patient's internal anatomy will move and deform during horizontal rotation as a result of gravity.

Buckley *et al.*[10] has shown that the magnitude of deformation during horizontal rotation can be large and techniques conventionally employed to account for target motion during radiotherapy such as margin expansion are unsuitable. For a compact fixed-beam treatment system to maintain dosimetric accuracy with a rotating patient, real-time image guidance must be incorporated into the treatment workflow[11]. The prototype PRS uses the Elekta Synergy's integrated kV imaging source to image the target during rotation, with custom software to record the geometry between imaging beam and target angle for each frame.

In this work, we demonstrate an image-guided treatment using the prototype fixed-beam system with a treatment workflow that is analogous to conventional radiotherapy. We have integrated two image guidance algorithms that allows the magnitude of target motion due to gravitational deformation to be measured during rotation. These algorithms are motion compensated cone-beam CT (CBCT) reconstruction[12] (labelled 1 in Figure 1) and real-time Kilovoltage Intrafraction Monitoring (KIM)[13]

(labelled 2 in Figure 1). Analogous to conventional radiotherapy, the motion compensated cone-beam CT algorithm was used to verify patient position prior to treatment delivery, while KIM measured the target position in real-time as the patient is rotated to each beam angle. At each treatment angle, the calculated target position from the two algorithms was then used to adapt the beam adaptation via the multi-leaf collimator (MLC) in order to maintain dosimetric accuracy. Using a custom designed deformable phantom, we performed an end-to-end treatment verification of this workflow comparing the dose delivered to a conventional rotating gantry treatment.

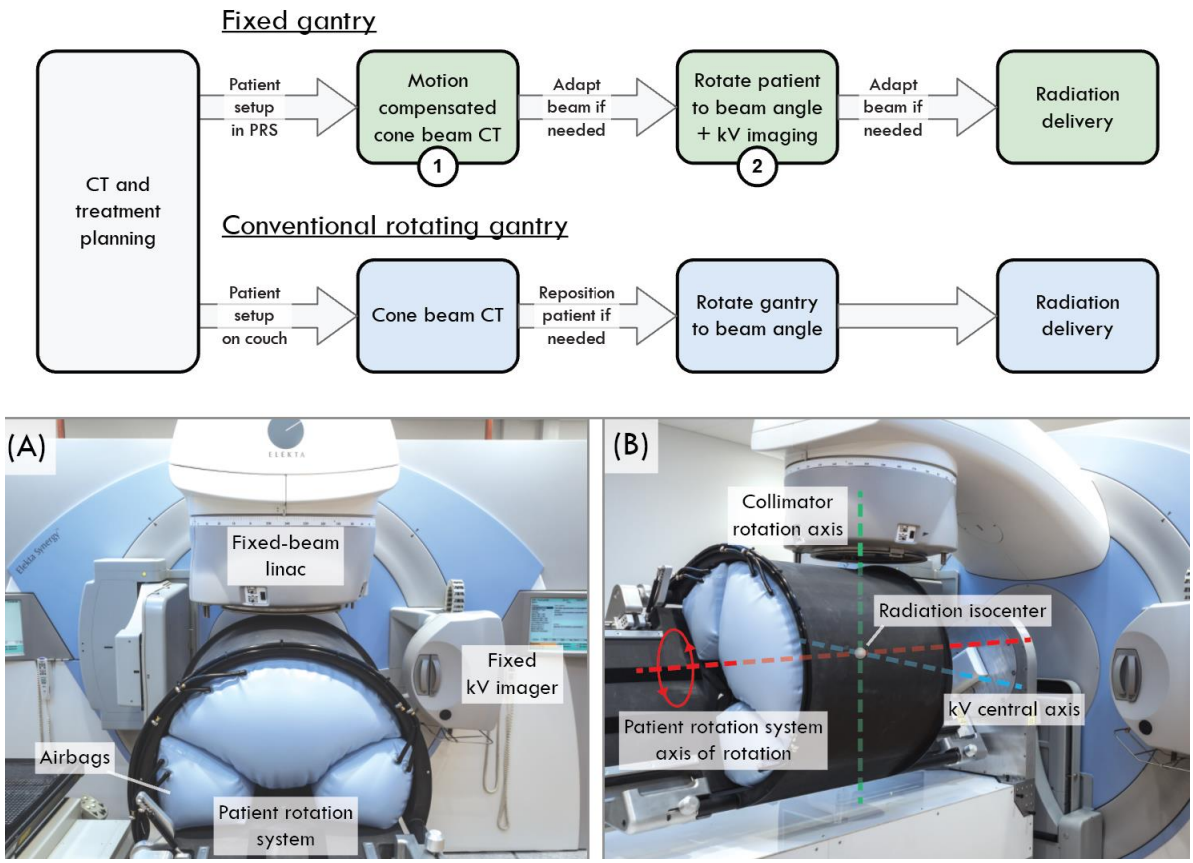

Figure 1 The end-to-end workflow for a motion-compensated fixed-beam treatment with a patient rotation system (PRS) compared to a treatment delivered on a conventional rotating gantry linac. The motion compensation algorithms utilized during fixed-beam delivery are (1) motion compensated cone beam CT reconstruction and (2) Kilovoltage Intrafraction Monitoring. Photo (A) shows the main components and photo (B) shows the geometric setup of the prototype fixed-beam treatment system.

Materials and Method

The prototype fixed-beam radiotherapy system consists of two major components: (1) a standard Elekta Synergy linac with gantry fixed at 0° and (2) a horizontal patient rotation system (Figure 1A). The patient rotation system (PRS) is a custom radiotherapy couch that replaces the conventional

couch. The PRS was installed such that its axis of rotation is perpendicular to the central beam axis of the linac and the central axis of the integrated kV imager, as shown in Figure 1B.

Design and construction of deformable phantom

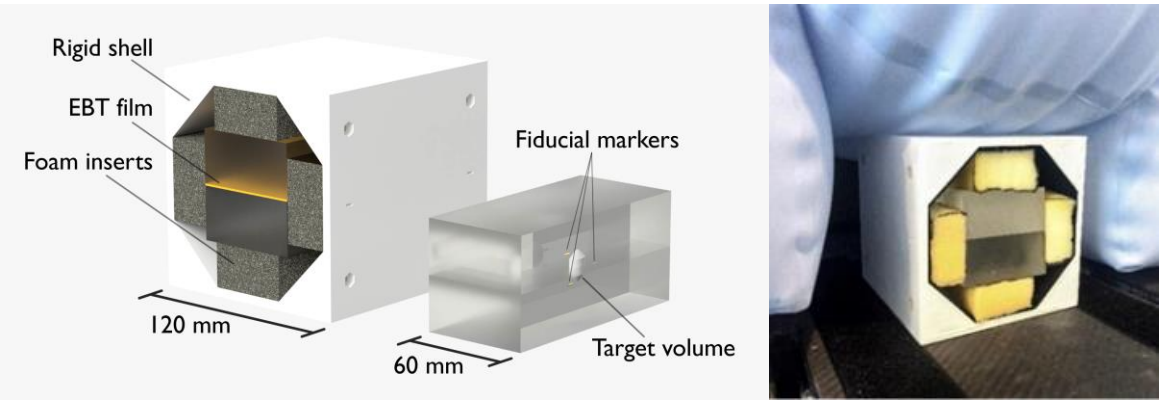

Figure 2 (A) Design and components of the deformable phantom and the acrylic insert (B) photograph of the deformable phantom immobilized in the PRS using airbags.

To quantify the geometric accuracy of the two image guidance methods as well as the overall dosimetric accuracy of the end-to-end treatment, a custom deformable phantom was constructed to imitate the anatomic motion of a patient under rotation. The design of the phantom is shown in Figure 2A. It consists of a cubic outer shell made of ABS plastic 120 mm in width and an acrylic insert 60 mm in width. An acrylic insert contains an epoxy tumor analogue surrounded by three gold fiducial markers (5 mm in length and 1 mm in diameter) and space for gafchromic EBT3 film (Ashland, Kentucky, US) for dosimetric measurements. The acrylic insert is held in the shell via deformable foam inserts. The foam inserts compress under gravity as the phantom is rotated, causing the acrylic insert to move as the angle of the phantom changes.

For phantom measurements, the outer shell was placed within the PRS by aligning the room lasers to markers on the exterior of the shell. The shell was then immobilized using the computer-controlled airbags at high air pressure. When the PRS is rotated, the outer shell remained mostly stationary while the inner acrylic insert was free to deform with gravity.

Pre-treatment verification using CBCT

As with conventional radiotherapy treatment, the fixed-beam treatment workflow utilizes a motion compensated cone-beam CT (CBCT) to verify target position prior to irradiation. This CBCT was performed with a full 360° rotation of the PRS at a constant velocity of 3 degrees per second while acquiring kV x-ray image projections using the integrated kV imager[9,14]. Images are streamed from

the XVi operating in fluoroscopy mode at 5.5 Hz for a total of 700 projections per scan. The imaging parameters used were 120 kVp, 25 mA and 40 ms. The projections were reconstructed to a 3D volume using a motion compensated reconstruction algorithm previously described by Shieh *et al.*[12] that accounts for gravity-induced motion during rotation to reduce motion blur in the image. The motion compensated CBCT reconstruction algorithms utilized the RTK reconstruction library[15] as well as the Elastix library[16] for rigid registrations. The voxel size was 0.8 mm and image dimension size was 512 × 512 × 512 pixels. Following reconstruction, the marker positions were manually delineated from the 3D volume and averaged to calculate the target position at 0°. The marker positions were compared to those measured using kV triangulation (described below) to quantify the geometric accuracy of the reconstruction algorithm.

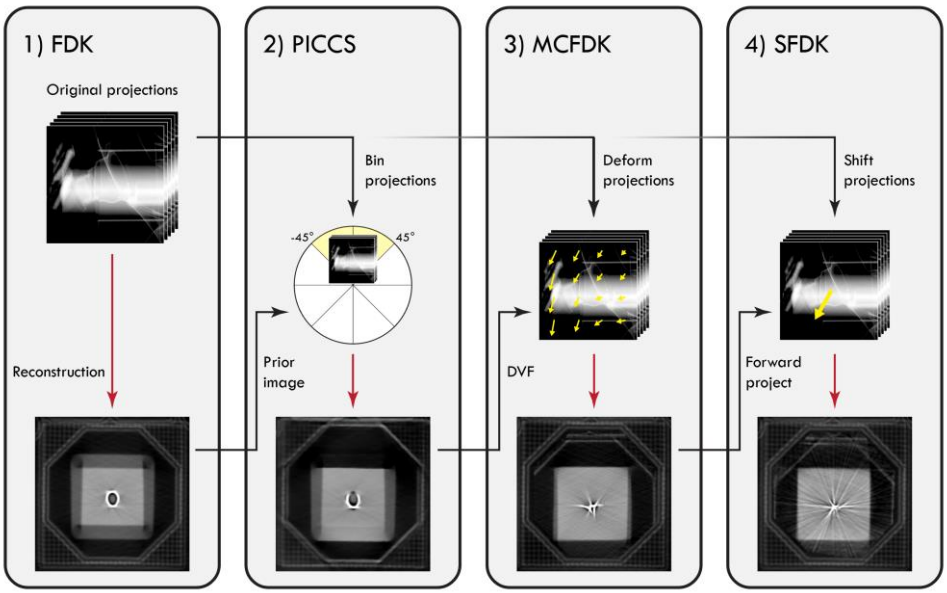

Figure 3 The workflow of the motion compensated CBCT algorithm and example transverse slices of the reconstructed volume at each stage of the reconstruction process for a phantom at 0°.

The motion compensated CBCT reconstruction algorithm consists of four stages to account for motion due to rotation and improve the reconstruction quality shown in Figure 3. (1) Feldkamp-Davis-Kress (FDK) reconstruction[17] using all projections to create a prior volume. (2) Prior image constrained compressed sensing (PICCS) reconstruction[18] where the projections were binned based on the angle of rotation of the phantom. A total of 8 bins, each with a 90° angular span and centered at 45° intervals, was chosen to balance the trade-off between depth information and rotational motion blur, both of which increase with a wider angular range and larger number of projections. A separate PICCS volume was generated for each bin using the FDK reconstruction from stage 1 as a prior volume. (3) Motion compensated FDK (MCFDK) reconstruction[19] where the original projections are warped using a deformation vector field (DVF). The DVF for each angle bin was calculated by

registering each PICCS volume from stage 2 to each other. (4) Shifted FDK (SFDK) reconstruction where for each angle at 45° intervals, a set of motion-corrected projections were computed by forward projecting the MCFDK volume and aligning the original projections to these forward projections. The shifted projections were then reconstructed into the final motion-corrected volume using the FDK algorithm.

In addition to improving the accuracy of marker localization, the motion compensated CBCT reconstruction algorithm also reduces the image blur of edges in the volume. In practice this would allow a more accurate CBCT to CT match for patient position verification. The image blur at each stage of the reconstruction algorithm was quantified using the normalized edge width, defined as the width of the edge transition from 20% to 80% of pixel values normalized between 0 and 1. To calculate the normalized edge width, the transverse slice of the reconstructed image through the center of the target was selected. On this slice, a line profile was taken for each of the four edges of the acrylic insert. The normalized edge width was calculated for each line profile and averaged.

Real-time target tracking using KIM

Kilovoltage Intrafraction Monitoring (KIM) is a fiducial marker based real-time tracking algorithm that calculates the 3D position of a target based on 2D x-ray projections taken using the gantry mounted integrated kV imager. The KIM workflow for a conventional rotating gantry system is detailed in Keall *et al.* [20]

The implementation of KIM with the prototype system was similar to the implementation using a miniature phantom rotation platform described in Liu *et al.* [21], where accurate target tracking was demonstrated as the phantom was rotated about the *z* (superior-inferior) axis, given that the axis of rotation is well aligned with the central axis of the kV imaging source. Prior to treatment delivery, a 3D probability density function (PDF) was fit to the 2D trajectories of the fiducial markers that was then used to estimate the maximum likelihood of 3D target position during treatment. The kV projections of the CBCT were used to construct the PDF for KIM.

During treatment delivery, kV fluoroscopic images are continuously acquired as the PRS is rotated to each beam angle. The angle of the PRS is input into the KIM software which calculates the real-time 3D position of the fiducial markers based on the angle, the three 2D marker positions on the images and the PDF.

Geometric accuracy of image guidance

The geometric accuracy of both image guidance methods was measured by comparing the calculated target position to the ground-truth position calculated using kV triangulation. kV triangulation was performed by rotating the gantry to two different angles (45° and 330°) and acquiring a single kV image. The pixel value of each marker at the two angles were recorded and the 3D marker position was calculated using the sequential stereo imaging method[22]. The three markers were averaged to calculate the 3D target position. The uncertainty of kV triangulation was estimated to be 1 pixel for each marker, which represents a distance of 0.8 mm at isocenter and a total uncertainty of 1.4 mm for the target position.

To measure the geometric accuracy of the motion compensated reconstruction algorithm, the deformable phantom was immobilized and rotated 360° for CBCT acquisition at three different locations: at isocenter, with a 21 mm shift in the *y* axis (patient's anterior at 0°) and with a -50 mm in the *x* axis (patient's left at 0°). At each location, kV triangulation was performed before and after the full CBCT rotation with the acquisition of kV images of the phantom at 0°. For each reconstructed CBCT volume, the locations of the three fiducial markers in the phantom were delineated and averaged to calculate the 3D target position that was compared to the ground-truth target position from the triangulation.

To measure the geometric accuracy of KIM, the deformable phantom was rotated to five discrete angles (0˚, 45˚, 135˚, 210˚ and 300˚) while KIM tracked the position of the target. At each of the five positions, the gantry of the linac was rotated from 0° to angles of 45° and 330° and a single kV image was acquired at each gantry angle for triangulation. The gantry was then rotated back to 0° to proceed to the next angle.

Fixed-beam MLC adaptation

Adaptation of the radiation beam to compensate for target motion and maintain dose coverage is performed prior to the delivery of each treatment field. For each treatment field, an in-house algorithm calculated new MLC leaf positions based on the position information provided using motion compensated CBCT and KIM.

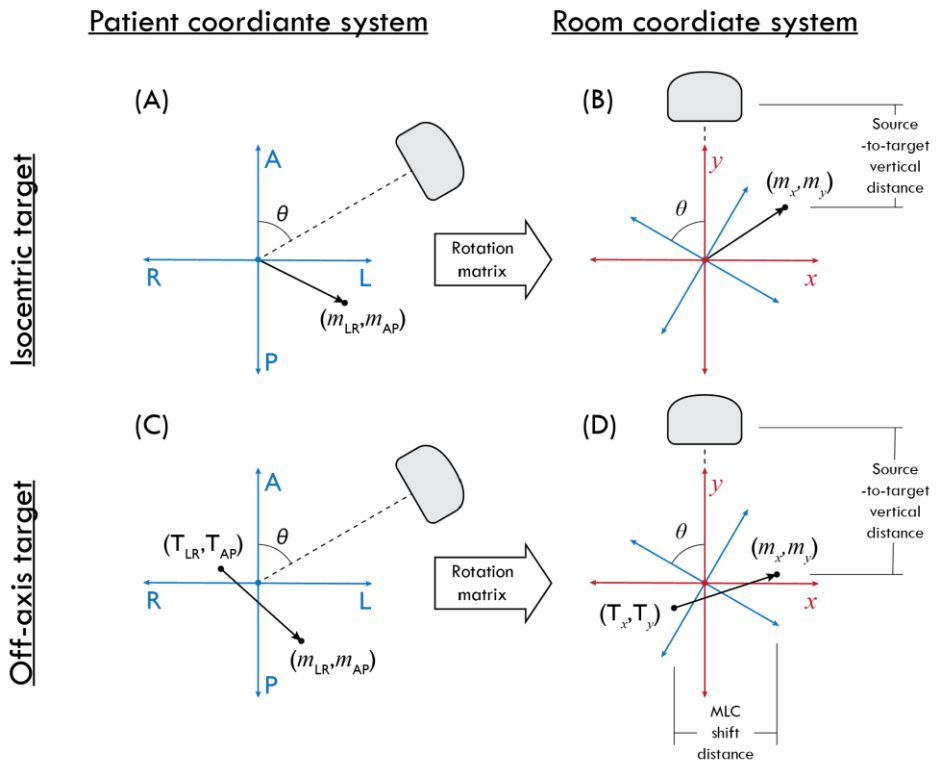

Figure 4 Transformations for target motion (vector *m*) from the patient coordinate system that would be used in conventional treatments with a rotating gantry to a room coordinate system used in fixed-beam treatments for gantry angle θ. Transformation from (A) to (B) is for a target at the isocenter and transformation from (C) to (D) is for an off-axis target initially located at point *T*.

To calculate the new leaf positions, the treatment plan and the target's motion are both transformed from the patient coordinate system, which assumes a normal head-first patient supine position with the axes LR, AP and SI to a room coordinate system, with axes *x*, *y* and *z*. For each treatment field, the target's motion during rotation is calculated using the image guidance methods described above and expressed as a 3D motion vector (*m*) in the patient coordinate system. The transformation, shown in Figure 4, is performed using the rotation matrix along the coincident SI or *z* axis for the couch angle θ:

$$\begin{pmatrix} m_x \\ m_y \\ m_z \end{pmatrix} = \begin{pmatrix} cos\ \theta & -sin\ \theta & 0 \\ sin\ \theta & cos\ \theta & 0 \\ 0 & 0 & 1 \end{pmatrix} \cdot \begin{pmatrix} m_{LR} \\ m_{AP} \\ m_{SI} \end{pmatrix}$$

For off-axis targets, the same rotation matrix is also used to transform the target centroid position (point *T* in Figure 4C, taken from the DICOM plan) to the room coordinate system, shown in Figure 2D. Off-axis treatments are more common with fixed-beam systems with patient rotation as the patient would always be set-up in a single position and beam adaption rather than patient repositioning would be used to align the beam.

The components of T and m along the x and y axis are used to calculate the necessary shift in the beam aperture. For simplicity, all treatments were planned with the collimator fixed at 0°, meaning the leaves of the MLC are always aligned with the x axis. Both the MLC leaves and the collimator jaws are shifted either left or right, as shown in Figure 4. The magnitude of the shift is determined by the distance m_x scaled by changes in the source-to-target vertical distance (T_y and M_y), calculated using the equation

$$Beam\ shift\ (mm) = m_x \times \frac{1000 - T_y - m_y}{1000}$$

where 1000 is the source-to-axis of rotation distance in millimeters.

Target motion along the SI or z axis is not affected by the fixed-beam geometry and therefore no transformations are needed. To compensate for it, a couch shift of distance $-m_z$ is employed to reposition the target.

Treatment planning, delivery and dosimetric verification workflow

The image guidance and beam adaptation methods were tested by performing an end-to-end irradiation of the deformable phantom and comparing to the planned dose. A CT scan of the deformable phantom was acquired and imported into the Elekta XiO v5.10 treatment planning system. A 6 MV x-ray 3D conformal treatment plan was planned with a PTV centered around the epoxy target in the acrylic insert. As the foam insert below the acrylic insert is compressed by gravity at 0˚, the target is located off-axis at approximately 8 mm below the isocenter. Four treatment fields at angles of 45˚, 135˚, 210˚ and 300˚ were planned. Custom software was used to convert these fields for the fixed-beam geometry by reading the treatment plan in DICOM format and recording the gantry angle and the coordinates of the target centroid for each treatment field. The original gantry angle of each control point is replaced with a new fixed angle of 0° and the new plan is exported as a DICOM file.

The workflow shown in Figure 1 was used to deliver the fixed-beam treatment. The deformable phantom was immobilized in the PRS and the initial position of the target was calculated using a motion compensated CBCT. The treatment fields and the treatment couch were adjusted accordingly. The images acquired during the CBCT were also used the input to KIM. As the PRS was rotated to each treatment angle, kV images continued to be acquired and KIM was used to calculate the real-time target position. At each treatment angle, the MLC leaves were adjusted based on Equation 2 to compensate for motion in the AP and LR axis and the treatment couch was moved to compensate for

motion in the SI axis. For comparison, the same treatment was also delivered without motion compensation on a Elekta Synergy linac with conventional rotating gantry delivery.

The dose delivered to the phantom's target in each case was measured using EBT3 film placed between the two halves of the tumor target, perpendicular to the beam central axis at gantry 0° and couch angle 0°. Film analysis was performed using the method described in Devic *et al.*[23] Each piece of EBT3 film was scanned prior to irradiation using an Epson 10000XL flatbed scanner (SEIKO Epson Co, Japan) in transmission mode with 48-bit RGB and a scanner resolution of 75 dpi. Following irradiation, the film was left for at least 24 h and scanned with identical settings. The ratio of red channel pixel values from the pre-irradiated film to the irradiated film was calculated for each pixel. The net optical density of each pixel was calculated by taking the log of this ratio then related to dose using a calibration curve relating optical density to dose obtained in the same measurement session. Dosimetric analysis compared to the planned dose was performed by analyzing in-plane and cross-plane dose profiles and by performing a 2D gamma analysis using a 3%/2 mm criteria[24], suppressing the dose for areas of the film receiving below 10% of the maximum dose.

Results

Geometric accuracy of motion compensated CBCT

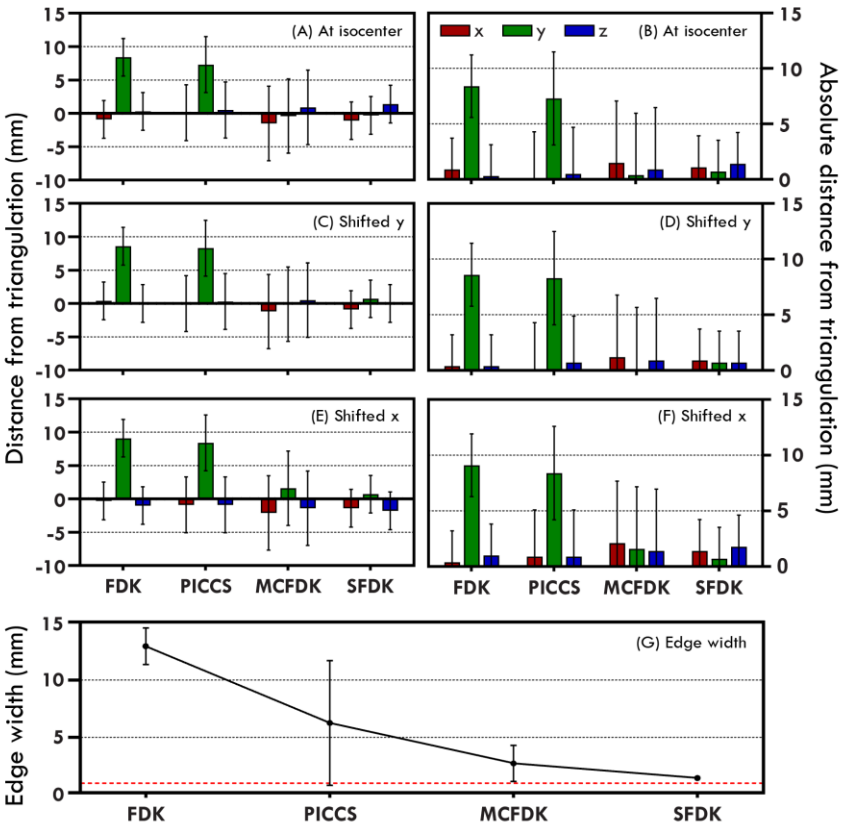

Figure 5 (A-F) The average difference and average absolute difference between the ground truth target position (calculated using triangulation) and the target position calculated with each stage of the motion compensated CBCT reconstruction algorithm for three phantom positions at 0˚. For each reconstruction step, error bars were calculated by adding uncertainty in marker localization due to noise, streaking artefacts and blurring in quadrature, then averaged across the three markers in the phantom. (G) The average edge width of the four sides of the phantom at each stage of the reconstruction algorithm. The red dotted line represents the edge width of the deformable phantom imaged with a conventional rotating gantry. Error bars represent the standard deviation of edge widths at the three slice positions containing markers.

Figure 3 shows an example transverse slice of the deformable phantom and a fiducial marker during each stage of the motion compensated CBCT reconstruction process. Using a FDK reconstruction, deformation during rotation caused the marker to appear as an annulus, the center of which was used as the estimated position of the marker. In the final shifted FDK image, the marker resembled streaking artifacts from a standard CBCT. In this case, the intersection of the streaks was used to estimate the position of the marker.

Figure 5A-F shows the average difference and average absolute difference in the position of the target calculated at each stage of the reconstruction process and the ground truth position calculated using triangulation. The FDK reconstruction accurately calculated the position of the target in the *x* and *z* directions (LR and SI in the patient coordinate system at 0˚) with an average difference of -0.3 mm and -0.2 mm respectively and an average absolute difference of 0.5 and 0.4 mm respectively. However, the average difference in the *y* axis (AP) was an average of 8.7 mm. Using the motion compensated CBCT reconstruction algorithm, the average differences in the *x*, y and *z* directions were -1.1 mm, 0.4 mm and -0.1 mm respectively with an average absolute difference of 1.1 mm, 0.6 mm and 1.1 mm respectively. This means the motion compensated CBCT reconstruction had greatly improved the accuracy of marker localization in the *y* axis where gravity induced motion is most evident.

Figure 5G shows the reduction in image blur at each stage of the reconstruction process. The average edge width (20% - 80%) of the phantom was reduced from 12.8 ± 1.6 mm with the FDK reconstruction to 1.4 ± 0.2 mm with the SFDK reconstruction. For comparison, CBCT images acquired with the same parameters with a conventional rotating gantry had an average edge width of 1.0 ± 0.1 mm.

Geometric accuracy of KIM

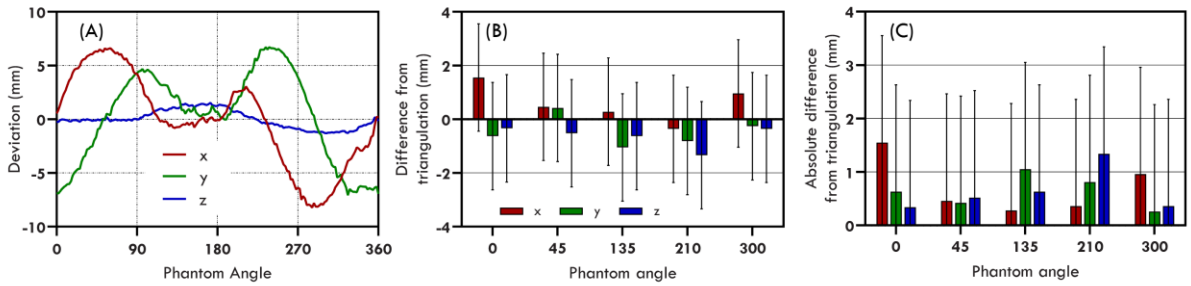

Figure 6 (A) The motion of the deformable phantom, expressed as deviation from the isocenter, over a full rotation in the PRS. (B and C) The difference and absolute difference between the ground truth target position (calculated using triangulation) and the target position calculated with KIM at 5 discrete angles. Error bars represent the standard deviation of the difference from triangulation over all kV frames collected when the phantom is rotated to discrete positions.

Figure 6A shows the average motion of the deformable phantom measured using KIM over six rotations in the PRS. The acrylic insert is shown to compress the foam, resulting in a sinusoidal motion in the patient's AP and LR directions. Figure 6A shows the sinusoids transformed to the fixed-beam coordinate system, with maximum average displacement of -8.2 mm, -7.1 mm and -1.3 mm in the *x*, *y* and *z* directions, respectively. The deformation of the phantom was different with each

rotation, with the target position varying by up to 3 mm. Figure 6B and 6C shows the position of the target measured in real-time using KIM compared to the ground truth position calculated using triangulation of two kV images. The average difference in the *x*, *y* and *z* directions was 0.6 mm, -0.5 mm and -0.6 mm respectively with an average absolute error of 0.7 mm, 0.6 mm and 0.6 mm respectively. The uncertainty of the KIM measurements was higher than sub-millimeter uncertainty of reported with a rotating gantry[25], resulting from imperfect alignment of the PRS axis of rotation to the kV central axis.

Dosimetric verification

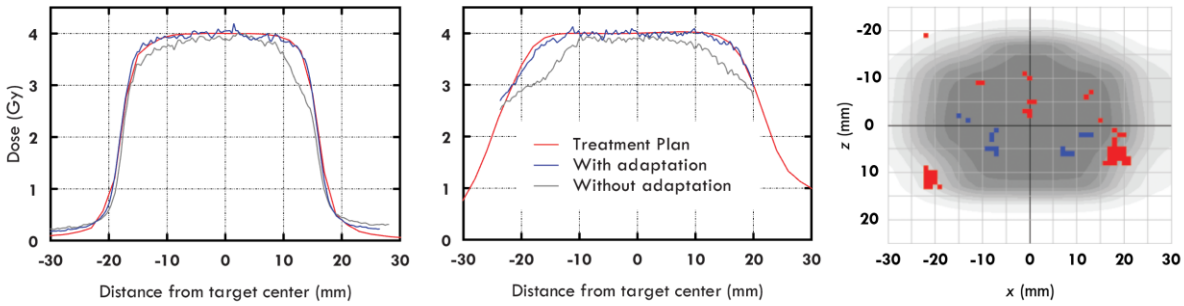

Figure 7 Inplane (left) and crossplane (center) dose profiles along the *z* and *x* axis (SI and LR axis in the patient's frame of reference at 0˚). Gamma analysis (global 3%/2mm, right) is shown comparing the delivered dose to the planned dose. Blue and red pixels represent failing areas of underdose and overdose respectively.

Figure 7 shows the measured dose distribution using image guidance and beam aperture shifts. The treatment fields at beam angles of 45˚, 135˚, 210˚ and 300˚ required aperture shifts of 4.1, 1.6, -7.4 and -10.9 mm respectively. The dose profiles of the motion compensated treatments showed good agreement with the dose profiles of the treatment plan. Gamma analysis using global 3%/2mm criteria is shown compared to the planned dose, with blue and red pixels representing failing areas of underdose and overdose respectively. The gamma pass rate for the real-time image guided treatment with a moving target was 96.3% compared to 80.9% without image guidance. The same treatment delivered conventionally with a rotating gantry to a static target resulted in a pass rate of 98.6%.

Discussion

A compact radiotherapy system with a fixed vertical beam and horizontal patient rotation has the advantages of fewer moving parts, smaller footprint and less shielding. The major challenges for such treatment system are anatomical deformation during rotation and patient acceptance of rotation. In this work, we have demonstrated the use of image guidance to address the first of these two challenges. We have implemented two methods that used a fixed kV source to acquire images of a deformable

phantom as it rotated and incorporated these methods in an end-to-end workflow for a 3D conformal treatment.

The motion compensated CBCT algorithm was shown to accurately calculate the position of the target at 0˚ and was used to confirm patient positioning in a manner similar to the role of CBCT in conventional rotating gantry radiotherapy. KIM was used to monitor target position in real-time during rotation and allowed the treatment beam to be adapted prior to irradiation to maintain target coverage. Using these two methods, we have shown the ability to maintain dosimetric accuracy during delivery of a 3D conformal treatment plan to a deformable phantom that moved up to 11 mm during rotation due to gravity. The accuracy of dose delivery was comparable to the accuracy when the treatment plan was delivered with a conventional rotating gantry linac.

The clinical driver for this work is the global need for more radiation therapy systems. As of 2020, there are 14,039 megavoltage radiotherapy units worldwide, while it is estimated that 21,800 units will be required by 2035 to meet demand[2,26]. As a result, there has been a severe under-utilization of radiotherapy around the world which will only worsen with time without significant investment in infrastructure. We have shown in a deformable phantom that the combination of target rotation and image guidance would allow radiotherapy to be accurately delivered using a compact treatment system with a fixed vertical megavoltage beam. Such a system would require less bunker shielding as the primary beam is shielded by the ground and would allow existing bunkers (such as those for cobalt-60 machines) to be used with a linac.

Despite the potential benefits in improving global access to treatment, there are still several challenges to widespread adoption of fixed-beam treatment systems. The tolerance of patients to motion during positioning, particularly horizontal rotation, has yet to be studied in depth. Sweeney *et al.*[27] showed that radiotherapy patients and volunteers on a robotic couch were unaffected whilst undergoing periodic motion. Whelan *et al.*[28] assessed the claustrophobia, anxiety and motion sickness of 15 patients during rotation at 12° s^{-1} and in either orientation, no significant differences were found in anxiety and motion sickness before and after rotation. To better understand this challenge, a clinical trial assessing the tolerance of radiotherapy patients to horizontal rotation in the PRS prototype is currently underway[29].

Another challenge is the nature of deformation for human patients. Due to size and weight, it is expected that the magnitude of deformation will be larger in humans than in the deformable phantom and in the rabbits imaged in Shieh *et al.*[12] where deformation was less than 15 mm. Buckley *et al.*[10] measured pelvic deformation during horizontal rotation to range from 5.8 ± 2.9 mm to 30.0 ± 11.0mm for healthy volunteers, most significantly in the left-right direction. Further investigation will be

required to scale and optimize the motion compensated CBCT algorithm for the larger and more complex deformations in human patients.

Although the motion compensated CBCT algorithm can be used without fiducial markers, the use of markers for real-time target tracking with KIM represents a potential roadblock for the use of compact systems in challenging environments. Fiducial markers are currently the gold standard for target localization in conventional radiotherapy[30,31], but their implantation is an invasive procedure that requires equipment and expertise. Despite this, image guidance algorithms such as KIM are beneficial in challenging environments as they can automate the patient setup procedure. KIM would reduce the expertise and time burden required during treatment to ensure that the patient is correctly aligned. The treatment beam could be automatically shifted in place of repositioning of the patient.

To avoid the reliance on implanted fiducial markers, marker-less tracking algorithms could be implemented for a fixed-beam system in a manner similar to that of KIM in this work. Marker-less tracking algorithms are under development for multiple treatment sites such as prostate[32] and lung[33] though there are currently no commercially available systems. Recent advances in deep learning have improved the speed and geometric accuracy of directly tracking the tumor, while the marker-less tracking of surrogates such as the diaphragm has also been shown to be an accurate alternative.[34] Marker-less tracking would be particularly beneficial in a low-cost system such as the fixed-beam protype. The increase in computational complexity would be offset by the reduction in linac complexity, bunker size and shielding requirements for a fixed beam system. Further development of mark-less tracking algorithms would be needed to account for the fixed-beam geometry and the potentially larger deformation resulting from patient rotation.

A further advancement for the prototype fixed-beam systems is the implementation of more advanced beam delivery and beam adaptation techniques. The treatment beam in this work was both delivered in a step-and-shoot approach, with each treatment field individually adapted via an MLC shift. The delivery of more complex treatment modalities such as IMRT or VMAT treatments that utilize slow continuous rotation will result in more complex dose distributions with greater conformality and normal tissue sparing. For these treatments, real-time beam adaptation via MLC tracking would be needed in place of discrete MLC shifts. MLC tracking reshapes the beam aperture in real-time to maintain coverage of the target volume. MLC tracking has been shown to be effectively combined with KIM for patient treatments on a conventional linac[35,36] and for fixed-beam treatments using a miniature phantom rotator[21]. Furthermore, current implementation of real-time beam adaptation techniques such as beam shifts on the CyberKnife, Vero, Radixact systems and MLC tracking on standard linear accelerators are first-order corrections that translate the beam to maintain target coverage. A second-order correction would also adapt the treatment plan based on changes to

anatomy, target depth and the dose delivered to nearby organs. Such a second-order correction would be a particularly important advancement in fixed-beam systems where large deformations can arise during rotation. The implementation of second-order corrections would require real-time dose reconstruction and evaluation during beam delivery, for example shown in Ravkilde *et al.*[37] , would enable MLC leaves to be reshaped depending on anatomic changes.

Conclusion

We have demonstrated the accurate delivery of 3D conformal radiotherapy to a deformable phantom with a prototype fixed-beam treatment system that utilizes target rotation instead of a gantry rotation. A fixed-beam treatment system can be made more compact and reliable than a conventional rotation gantry system, however, the horizontal rotation of a patient could cause anatomical deformation during treatment. We have incorporated two image guidance algorithms that compensate for deformation during rotation to maintain dosimetric accuracy.

Acknowledgements

The authors acknowledge the Sydney Informatics Hub and the University of Sydney's high performance computing cluster Artemis for providing the high performance computing resources that have contributed to the research results reported within this paper. PL, DN and RO acknowledge funding from Cancer Institute NSW fellowships. DN acknowledges funding from an NHMRC early career fellowship. PJK acknowledges the Australian Government NHMRC Senior Principal Research Fellowship. This research was partially funded by an NHMRC Development Grant.

References

1. Barton MB, Jacob S, Shafiq J, et al. Estimating the demand for radiotherapy from the evidence: a review of changes from 2003 to 2012 *Radiother Oncol.* 2014;112(1):140-144.
2. Atun R, Jaffray DA, Barton MB, et al. Expanding global access to radiotherapy *Lancet Oncol.* 2015;16(10):1153-1186.
3. Rosenblatt E, Zubizarreta E. *Radiotherapy in Cancer Care: Facing the Global Challenge.* Vienna: IAEA; 2017.
4. Van Dyk J, Zubizarreta E, Lievens Y. Cost evaluation to optimise radiation therapy implementation in different income settings: A time-driven activity-based analysis *Radiother Oncol.* 2017;125(2):178-185.
5. Pella A, Riboldi M, Tagaste B, et al. Commissioning and quality assurance of an integrated system for patient positioning and setup verification in particle therapy *Technol Cancer Res Treat.* 2014;13(4):303-314.
6. Wang N, Ghebremedhin A, Patyal B. Commissioning of a proton gantry equipped with dual x-ray imagers and a robotic patient positioner, and evaluation of the accuracy of single-beam image registration for this system *Med Phys.* 2015;42(6):2979-2991.
7. Eslick EM, Keall PJ. The Nano-X Linear Accelerator: A Compact and Economical Cancer Radiotherapy System Incorporating Patient Rotation *Technol Cancer Res Treat.* 2015;14(5):565-572.

8. Feain I, Coleman L, Wallis H, Sokolov R, O'Brien R, Keall P. Technical Note: The design and function of a horizontal patient rotation system for the purposes of fixed-beam cancer radiotherapy *Med Phys.* 2017;44(6):2490-2502.
9. Liu PZY, O'Brien R, Heng SM, et al. Development and commissioning of a full-size prototype fixed-beam radiotherapy system with horizontal patient rotation *Med Phys.* 2019;46(3):1331-1340.
10. Buckley JG, Rai R, Liney GP, et al. Anatomical deformation due to horizontal rotation: towards gantry-free radiation therapy *Phys Med Biol.* 2019;64(17):175014.
11. Kairn T. Patient rotation during linac-based photon electron radiotherapy *J Med Imaging Radiat Oncol.* 2018. doi: 10.1111/1754-9485.12757.
12. Shieh CC, Barber J, Counter W, et al. Cone-beam CT reconstruction with gravity-induced motion *Phys Med Biol.* 2018. doi: 10.1088/1361-6560/aae1bb.
13. Keall PJ, Aun Ng J, O'Brien R, et al. The first clinical treatment with kilovoltage intrafraction monitoring (KIM): a real-time image guidance method *Med Phys.* 2015;42(1):354-358.
14. Feain I, Shieh CC, White P, et al. Functional imaging equivalence and proof of concept for image-guided adaptive radiotherapy with fixed gantry and rotating couch *Adv Radiat Oncol.* 2016;1(4):365-372.
15. Rit S, Oliva MV, Brousmiche S, Labarbe R, Sarrut D, Sharp GC. The Reconstruction Toolkit (RTK), an open-source cone-beam CT reconstruction toolkit based on the Insight Toolkit (ITK). Paper presented at: J Phys Conf Ser2014.
16. Klein S, Staring M, Murphy K, Viergever MA, Pluim JP. elastix: a toolbox for intensity-based medical image registration *IEEE Trans Med Imaging.* 2010;29(1):196-205.
17. Feldkamp LA, Davis LC, Kress JW. Practical Cone-Beam Algorithm *J Opt Soc Am A.* 1984;1(6):612-619.
18. Chen GH, Tang J, Leng S. Prior image constrained compressed sensing (PICCS): a method to accurately reconstruct dynamic CT images from highly undersampled projection data sets *Med Phys.* 2008;35(2):660-663.
19. Rit S, Wolthaus JW, van Herk M, Sonke JJ. On-the-fly motion-compensated cone-beam CT using an a priori model of the respiratory motion *Med Phys.* 2009;36(6):2283-2296.
20. Keall PJ, Ng JA, Juneja P, et al. Real-Time 3D Image Guidance Using a Standard LINAC: Measured Motion, Accuracy, and Precision of the First Prospective Clinical Trial of Kilovoltage Intrafraction Monitoring-Guided Gating for Prostate Cancer Radiation Therapy *Int J Radiat Oncol Biol Phys.* 2016;94(5):1015-1021.
21. Liu PZY, Nguyen DT, Feain I, O'Brien R, Keall P, Booth JT. Technical note: Real-time image-guided adaptive radiotherapy of a rigid target for a prototype fixed beam radiotherapy system *Med Phys.* 2018. doi: 10.1002/mp.13143.
22. Mostafavi H, Sloutsky A, Inventors. Sequential stereo imaging for estimating trajectory and monitoring target position. US patent 8396248B2 2013.
23. Devic S, Seuntjens J, Sham E, et al. Precise radiochromic film dosimetry using a flat-bed document scanner *Med Phys.* 2005;32(7):2245-2253.
24. Miften M, Olch A, Mihailidis D, et al. Tolerance limits and methodologies for IMRT measurement-based verification QA: Recommendations of AAPM Task Group No. 218 *Med Phys.* 2018;45(4):e53-e83.
25. Kim JH, Nguyen DT, Huang CY, et al. Quantifying the accuracy and precision of a novel real-time 6 degree-of-freedom kilovoltage intrafraction monitoring (KIM) target tracking system *Phys Med Biol.* 2017;62(14):5744-5759.
26. Agency IAE. *Directory of Radiotherapy Centres*. https://nucleus.iaea.org/Pages/dirac.aspx. Accessed September 2018.
27. Sweeney RA, Arnold W, Steixner E, Nevinny-Stickel M, Lukas P. Compensating for tumor motion by a 6-degree-of-freedom treatment couch: is patient tolerance an issue? *Int J Radiat Oncol Biol Phys.* 2009;74(1):168-171.
28. Whelan B, Welgampola M, McGarvie L, et al. Patient reported outcomes of slow, single arc rotation: Do we need rotating gantries? *J Med Imaging Radiat Oncol.* 2017. doi: 10.1111/1754-9485.12688.

29. Debrot E, Liu P, Whelan B, et al. Will Patients Accept Horizontal Rotation During Radiotherapy Treatment? Patient Reported Outcomes of Rotation On a Prototype Fixed Beam Radiotherapy System. Paper presented at: American Association of Physicists in Medicine Annual Meeting 2020.
30. Ghadjar P, Fiorino C, Munck Af Rosenschold P, Pinkawa M, Zilli T, van der Heide UA. ESTRO ACROP consensus guideline on the use of image guided radiation therapy for localized prostate cancer *Radiother Oncol.* 2019;141:5-13.
31. Scher N, Bollet M, Bouilhol G, et al. Safety and efficacy of fiducial marker implantation for robotic stereotactic body radiation therapy with fiducial tracking *Radiat Oncol.* 2019;14(1):167.
32. Zhao W, Han B, Yang Y, et al. Toward Markerless Image-Guided Radiotherapy Using Deep Learning for Prostate Cancer. Paper presented at: Workshop on Artificial Intelligence in Radiation Therapy2019.
33. Hazelaar C, Dahele M, Mostafavi H, van der Weide L, Slotman B, Verbakel W. Markerless positional verification using template matching and triangulation of kV images acquired during irradiation for lung tumors treated in breath-hold *Phys Med Biol.* 2018;63(11):115005.
34. Hindley N, Keall P, Booth J, Shieh CC. Real-time direct diaphragm tracking using kV imaging on a standard linear accelerator *Med Phys.* 2019;46(10):4481-4489.
35. Hewson EA, Nguyen DT, O'Brien R, et al. Is multileaf collimator tracking or gating a better intrafraction motion adaptation strategy? An analysis of the TROG 15.01 Stereotactic Prostate Ablative Radiotherapy with KIM (SPARK) trial *Radiother Oncol.* 2020. doi: 10.1016/j.radonc.2020.08.010.
36. Keall P, Booth J, Nguyen DT, et al. The First Clinical Implementation of Real-time Adaptive Radiation Therapy Using a Standard Linear Accelerator *International Journal of Radiation Oncology • Biology • Physics.* 2017;99(2):S223-S224.
37. Ravkilde T, Skouboe S, Hansen R, Worm E, Poulsen PR. First online real-time evaluation of motion-induced 4D dose errors during radiotherapy delivery *Med Phys.* 2018. doi: 10.1002/mp.13037.